Space Weather

RESEARCH ARTICLE
10.1029/2019SW002421

# Differential Magnetometer Measurements of Geomagnetically Induced Currents in a Complex High Voltage Network

J. Hübert[1], C. D. Beggan[1], G. S. Richardson[1], T. Martyn[1], and A. W. P. Thomson[1]

[1]British Geological Survey, Edinburgh, UK

**Key Points:**
- Geomagnetically induced currents are measured in high voltage lines using the differential magnetometer method
- Line currents are compared with measurements from a transformer Hall probe at a local substation
- Measurements are compared with modeled line currents from a network representation

**Supporting Information:**
- Supporting Information S1

**Correspondence to:**
J. Hübert,
juliane.huebert@bgs.ac.uk

**Citation:**
Hübert, J., Beggan, C. D., Richardson, G. S., Martyn, T., & Thomson, A. W. P. (2020). Differential magnetometer measurements of geomagnetically induced currents in a complex high voltage network. *Space Weather*, *18*, e2019SW002421. https://doi.org/10.1029/2019SW002421

Received 29 NOV 2019
Accepted 2 MAR 2020
Accepted article online 4 MAR 2020



**Abstract** Space weather poses a hazard to grounded electrical infrastructure such as high voltage (HV) transformers, through the induction of geomagnetically induced currents (GICs). Modeling GICs requires knowledge of the source magnetic field and the Earth's electrical conductivity structure, in order to calculate the geoelectric fields generated during magnetic storms, as well as knowledge of the topology of the HV network. Direct measurement of GICs at the ground neutral in substations is possible with a Hall effect probe, but such data are not widely available. To validate our HV network model, we use the differential magnetometer method (DMM) to measure GICs in the 400 kV grid of Great Britain. We present DMM measurements for the 26 August 2018 storm at a site in eastern Scotland with up to 20 A recorded. The line GIC correlates well with Hall probe measurements at a local transformer, though they differ in amplitude by an order of magnitude (a maximum of ~2 A). We deployed a long-period magnetotelluric (MT) instrument to derive the local impedance tensor which can be used to predict the geoelectric field from the recorded magnetic field. Using the MT-derived electric field estimates, we model GICs within the network, accounting for the difference in magnitude between the DMM-measured line currents and earth currents at the local substation. We find that the measured line and earth GICs match the expected GICs from our network model, confirming that detailed knowledge of the complex network topology and its resistance parameters is essential for accurately computing GICs.

**Plain Language Summary** Large geomagnetic storms create time-varying magnetic fields, which induce secondary electric fields in the conductive Earth resulting in geomagnetically induced currents (GICs). The high voltage (HV) power transmission network is connected to the Earth at grounding points in substations. These offer a low-resistance path for GICs to flow into the power network, potentially causing the transformers to malfunction. It is possible to directly measure GICs at substations using Hall effect probes, but due to cost and operational reasons, at present only four substations in the United Kingdom are monitored. Therefore, we have developed a new instrument to measure GICs indirectly using two magnetometers, one placed under the HV line and another a few hundred meters away. By examining the differences between the magnetometers, we work out the additional current flowing in the HV line. We compare our measurements to observations made by a Hall probe at a nearby transformer during a geomagnetic storm in August 2018. The GICs from the line measurements match the shape of the Hall probe, but there is a difference in amplitude. Further analysis shows that the amplitude differences arise from the resistance and earthing properties of the individual HV lines and transformers within the power network.

## 1. Introduction

During severe space weather events, geomagnetic storm conditions arise when the Earth's magnetic field becomes strongly disturbed. Rapid variations in the magnetic field induce electric fields in the ground that depend on the underlying electrical conductivity structure. The complex temporal and spatial magnetic field variations cause differences in the electric field to arise over large areas, which can be up to several tens of V/km (Love et al., 2018; Myllys et al., 2014). The development of modern low-resistance ground infrastructure such as the high voltage (HV) power transmission network, gas pipelines, and railways allows the electric field to equalize through the earthing points of these conductors; the additional quasi steady DC currents are known as geomagnetically induced currents (GICs). This phenomenon is a threat to the optimal performance and operation of HV transformers (Albertson et al., 1981; Boteler, 2006; Pulkkinen et al., 2012).

A well-known example is the collapse of a Quebec-Hydro network in March 1989, attributed to the effects of large GICs (Bolduc, 2002; Boteler, 2019). The present-day cost of a widespread power outage has been estimated in the billions of U.S. dollars per day for advanced economies (e.g., Oughton et al., 2017, 2018).

A large number of studies modeling GICs in different HV networks have been published in the past decade. The key components for modeling GICs are (1) the computation of the geoelectric field from magnetic field variation observations coupled to an electrical conductivity model of the region (e.g., Divett et al., 2018; Kelbert et al., 2017; McKay, 2003; Pulkkinen et al., 2006) and (2) an accurate representation of the HV transmission system, including information about the network resistances (of grounding, transformer, and line) as well as the location of the substation earthing points and the paths of the connecting power lines (e.g., Torta et al., 2017; Turnbull, 2010; Viljanen et al., 2014). In the United Kingdom, research on space weather and its impact on ground-based infrastructure has been ongoing for over two decades. This has included research into the geophysical conditions which give rise to GICs, refining the regional conductivity of the subsurface and investigating extreme scenarios (Beamish et al., 2002; Beggan, 2015; Kelly et al., 2017; Thomson et al., 2005).

GIC flow in the network as a whole is dependent on the overall grid topology. Several mathematical approaches are used to compute GICs flowing through the network (assuming a quasi-DC current) using Ohm's law to estimate the strength of electrical currents entering and exiting substation grounding points (Boteler & Pirjola, 2014; Lehtinen & Pirjola, 1985). Recent improvements to GIC modeling codes (following Divett et al., 2018) allow the extraction of line currents, bus voltages, and individual transformer currents as well as net substation GICs. This code has been validated against the benchmark model of Horton et al. (2012). However, validating GICs in a HV model of a national grid against real-world measurements is generally more difficult.

Direct measurements of GICs can be made using a Hall effect probe clamped to the earth neutral in a substation, but these devices are expensive to install and maintain across a large network and are therefore uncommon. A more economical approach is to model GIC effects on a network and validate the estimates with spot measurements. To date, Hall effect probe measurements are only available at a few locations for a small number of HV networks (e.g., Bailey et al., 2018; Blake et al., 2018; Butala et al., 2017; Rosenqvist & Hall, 2019; Thomson et al., 2005), with the notable exception of the South Island of New Zealand where over 50 GIC monitoring sites are currently installed (Mac Manus et al., 2017; Marshall et al., 2012). In general, the scarceness of direct GIC measurements makes the validation of numerical network models quite challenging, especially when attempting to match data from only a small number of sites which themselves may not be representative of the network as a whole.

Indirect measurements of GICs are also possible. For example, the differential magnetometer method (DMM) was first applied to pipelines by Campbell (1980) and Pulkkinen et al. (2001) and adapted later for HV power lines (Matandirotya et al., 2016; Viljanen & Pirjola, 1994). With DMM, a magnetometer placed under a HV line detects the background magnetic field plus the excess quasi-DC current flow during strong geomagnetic activity, while the magnetic field measured at a remote site records only the natural variation. The difference can be used to compute the value of GICs in the line via Ampère's law. Another indirect approach is described in Clilverd et al. (2018) who correlated VLF emissions from a transformer with the occurrence of GICs. These methods have the advantage of being relatively inexpensive, easy to install, and require only passive measurements to be made, though additional effort is required to extract the absolute (rather than relative) value of GIC magnitude.

With only four Hall effect probes presently operating in the United Kingdom (Thomson et al., 2005), there are few directly measured GIC data available to validate the mainland Britain model. Therefore, we have sought indirect methods to measure GICs. In this study we present the first results from a field campaign to measure line GICs across the 400 kV network of mainland Britain using the DMM. We describe the hardware system and the deployment in the field at sites along the east coast of Britain and provide the results from our first DMM site in the east of Scotland for a geomagnetic storm on 26 August 2018. In support of research into space weather hazards, we also deployed a long-period magnetotelluric (MT) instrument to ascertain the local transfer function between magnetic and electric field variations.

In the following we describe the DMM systems, deployment, and modeling approach to compute the GICs flowing in the power lines. We show results from the DMM system for a geomagnetic storm. To put the

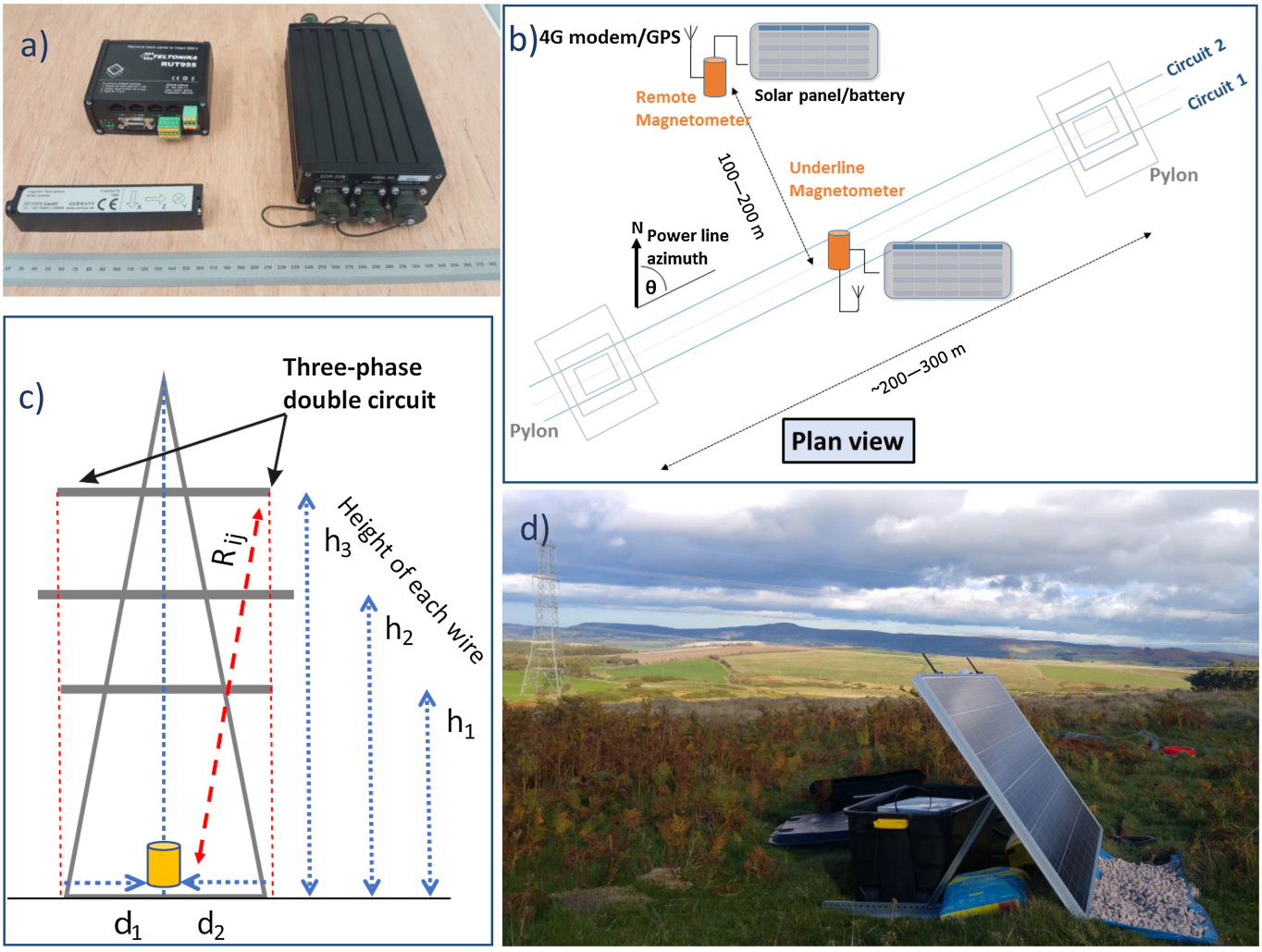


**Figure 1.** Hardware components of differential magnetometer system and field setup. (a) 4G mobile network modem, EarthData digitizer, fluxgate magnetometer (clockwise from top left). (b) Schematic plan view of underline and remote systems at a DMM site. (c) Geometry for sensor location and the wires in the double-circuit A-frame pylon model. (d) Photo of the remote station at Ilderton (ILD), Northumberland, with buried sensor, solar panel, and mobile network aerials, located 300 m from the 400 kV line seen in the background.

measured data in context, we provide information gathered from an MT survey and show the response of the network to a hypothetical 1 V/km geoelectric field. Finally, we compare the line GICs and measurements from a local substation Hall probe with GIC values obtained from a network model.

## 2. The Differential Magnetometer Method

In previous DMM studies, relatively simple system configurations were chosen for DMM measurements, making the computation of the expected GIC straightforward. Campbell (1980) measured current flowing in the single trans-Alaska high pressure gas pipeline, while the Viljanen and Pirjola (1994) study was based on a basic representation of the Finnish network. The study of Matandirotya et al. (2016) demonstrated the application of the DMM on a single three-phase HV line running through a remote area in Namibia. The authors used a LEMI-011 magnetometer to record the magnetic field variations under the line and compared it to data from a remote system placed around 200 m away. The system could detect GIC variations of less than 0.1 A.

The GB power transmission network, operated by National Grid UK plc, is much more complex, consisting of thousands of km of 400, 275, and 132 kV lines. It is highly interconnected, typically with three-phase double circuits on A-frame pylons, and transmits energy from the outer regions toward the densely populated

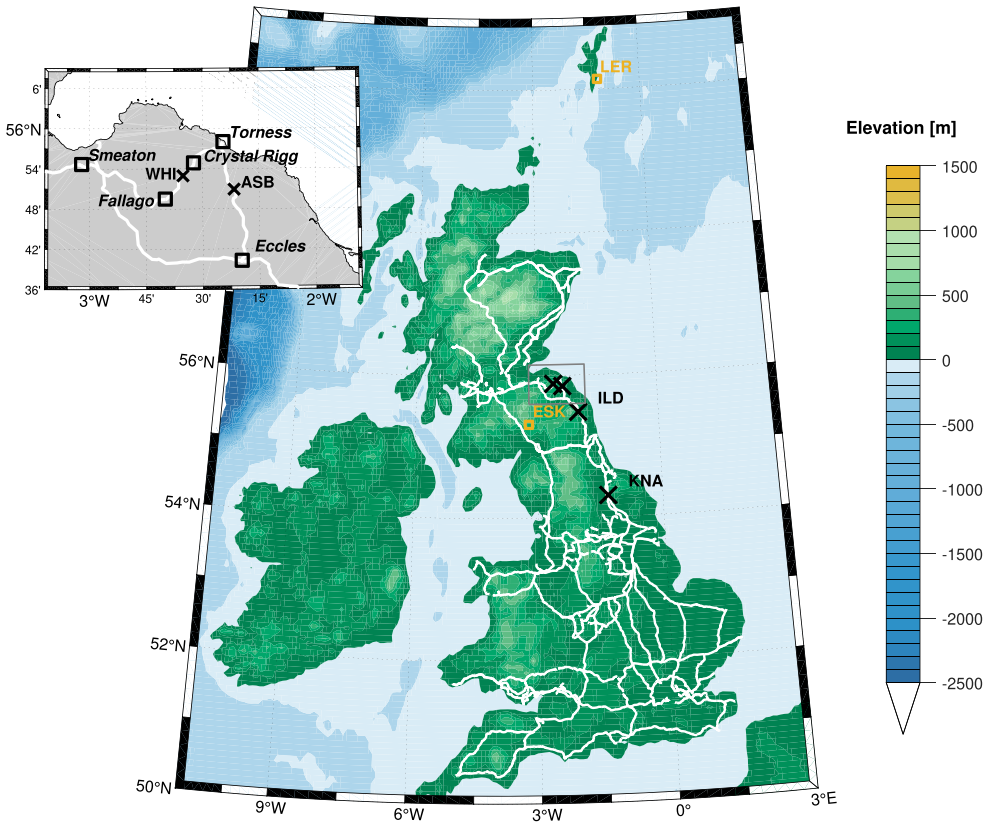


**Figure 2.** The 400 and 275 kV transmission network (white lines) and location of DMM systems deployed in 2018 (black crosses, WHI: Whiteadder; ASB: Abbey St. Bathans; ILD: Ilderton; KNA: Knayton) and geomagnetic observatories (orange squares, LER: Lerwick; ESK: Eskdalemuir). Inset shows the location of the substations (black squares) and DMM sites near Torness power station (in eastern Scotland).

areas in the south of England. This makes it much more complicated to model GICs and reconcile them with DMM observations compared to a single three-phase line, such as studied in Namibia.

### 2.1. Design and Deployment of the Differential Magnetometer Systems

Based on the principles described in Matandirotya et al. (2016), we developed a set of bespoke differential magnetometer systems. The design for each system (pairing an underline and a remote site) comprises a Sensys FGM3D triaxial fluxgate magnetometer combined with an Earth Data EDR209 three-channel digitizer (Figure 1a). The magnetic field data are transmitted in near real time (every 30 min) via a router using the 4G mobile phone network to the BGS office. The system is powered by two 90 Ah batteries, recharged by a 270 W solar panel. The remote data collection system is based on the well-established and robust IRIS SeedLink protocol (FDSN, 2012). Three data channels (magnetic north $B_x$, magnetic east $B_y$, and downward component $B_z$) are recorded at a 1 Hz sampling rate. Two auxiliary channels are used to monitor the battery voltage and the temperature from a thermistor close to the magnetic sensor. Accurate timing is guaranteed by a GPS antenna. The system was found to have a noise floor of 0.02 nT·Hz$^{1/2}$ within the frequency band of 0.1–0.5 Hz (period of 2–10 s).

When deployed in the field, the magnetic sensor is placed in a plastic barrel into which a wooden mount embedded in nonferrous concrete has been set. The barrel is buried and covered with insulation material to improve temperature stability over periods of several hours. The solar panel, digitizer, and the remaining electrical components are placed in a box around 8 m away from the sensor to reduce interference (Figure 1b). The magnetometer is leveled and orientated to magnetic North by nulling the east component of the horizontal field. Prior to the deployment, each pair of sensors and digitizer was calibrated together at the absolute pillar of the INTERMAGNET-standard Eskdalemuir Observatory (see Figure 2). We built 12 identical systems, allowing for up to six DMM sites to be recording simultaneously. Figure 1d shows the equipment deployed under a 400 kV power line near Ilderton (ILD), Northumberland.

We initially chose lines that the HV network model suggested would experience high GICs during geomagnetic storms, based on the work of Kelly et al. (2017). The underline sensor was placed under the lowest hanging point of the wires, midway between pylons, which are usually around 300 m apart. Figure 2 shows the field locations deployed during 2018. A further four sites were deployed in 2019.

### 2.2. Deriving GICs with the DMM

Following the approach of Matandirotya et al. (2016), we derive the line current $I$ from the magnetic field measurements $B$ observed at a distance $R$ from a single wire, assuming the Biot-Savart law for an infinite conductor:

$$B = \frac{\mu_0 I}{2\pi R}. \tag{1}$$

In the field the two triaxial fluxgate magnetometers are oriented in geomagnetic coordinates. To retrieve the signal corresponding to the excess current flowing in the power lines, the horizontal components of the recorded magnetic field at both the underline and remote station are rotated into a coordinate system parallel to the power lines. The difference between the underline and remote site in the magnetic field component transverse to the HV wires then maximizes the magnetic signal due to GICs in the line. Some signal detrending (or band-pass filtering) is required to account for long-period temperature effects and/or static offsets between the underline and remote sensors.

In contrast to the simple three-phase single circuit 66 kV HV line studied in Namibia, the configuration of 400 kV HV power lines in Britain is far more complex, typically with two double circuits, each consisting of two to four bundled wires supported by A-frame pylons (see Figures 1b and 1c). The line heights vary depending on topography and land use but typically lie in the range of 12–15 m for the lowest to 30–33 m for the upper wires. Precise measurement of line heights and widths is made with a Leica laser distance meter at each site. To account for the distances to each line in the double circuit, a model was created to invert for the GICs using the Biot-Savart law. Assuming that the GICs are quasi-static over a period of several seconds, we can treat each of the six wire bundles as an infinite conductor. If we further assume that both circuits are carrying equal current (or equivalently, each phase carries the same current) and connect to the same transformers at each end, we can describe the measured magnetic field as $B_{meas} = \sum_j B_j$, where $j = [1, 2]$ is the number of circuits. The contribution to the measured magnetic field from each wire on the A-frame pylon is

$$B = \sum_{j}^{2} \sum_{i}^{3} \frac{\mu_0 I}{3 \cdot 2\pi R_{ij}}, \tag{2}$$

where $i = [1, 2, 3]$ is the number of phases and $R_{ij} = \sqrt{(h_i^2 + d_j^2)}$ is the distance from the underline sensor to each wire bundle (Figure 1c). The average current flowing in the lines can now be estimated with

$$I = \sum_{j}^{2} \frac{B_j 6\pi R_{1j} R_{2j} R_{3j}}{\mu_0 (R_{1j} R_{2j} + R_{1j} R_{3j} + R_{2j} R_{3j})}. \tag{3}$$

If the circuits are unbalanced (i.e., each circuit is connected to a different transformer), the calculation of line GICs can be altered to accommodate this scenario. This can be achieved by calculating the contribution from each circuit ($j$) separately.

Prior to deployment, a sensitivity analysis, similar to that of Matandirotya et al. (2016), was carried out by varying the setup parameters such as the line height, ground conductivity, GIC magnitude, and the alignment of the DMM sensors, demonstrating that a sensitivity to GIC variations of around 0.1 A was achievable in theory. The analysis furthermore showed that at a distance of 100 m or greater, the remote system should measure less than 1% of the magnetic field created by GICs in the power line.

The main uncertainties in DMM measurements are a combination of absolute and relative errors, where the latter scale with the amplitude of the line GIC. Uncertainties caused by the installation are relative errors and include the uncertainty during the alignment of the sensors and estimating the position of the sensor in respect to the wires. Additionally, there is a small signal in the remote magnetometer from GIC flowing in the HV line.

The noise threshold of the fluxgate magnetometer is 0.1 nT and constitutes an absolute error. During the installation, the underline and remote sensors are co-aligned by precise leveling and minimizing the magnetic east component to within 5 nT. This is the alignment uncertainty. The underline sensor is placed either centrally between the double circuit (usually at 9 m horizontal distance) or directly under one line.

The positioning uncertainty derives from any error in measuring the distance to the wires. The distance between the overhead wires and the sensor is typically well constrained by using a laser range finder, and measurement errors should not exceed 0.5 m. This gives an uncertainty of up to 5% for wires at a height of 10 m, falling to around 1% for wires at 30 m. The magnetic effect of GICs flowing in the line as measured at 100 m distance is around 0.75% falling to 0.25% at 200 m.

As an example, assuming that a 10 A GIC flow in a HV line generates a 200 nT magnetic field measured at the underline sensor, with a remote station at 200 m, the root-sum-square calculation of uncertainty is 0.1 nT from the sensor, 5 nT from misalignment between remote and underline, 1.5 nT from the GIC effect at the remote, and 1.5 nT due to positioning uncertainty of underline sensor for a 0.5 m error: $\sqrt{(0.1^2 + 5^2 + 1.5^2 + 1.5^2)} = 5.4$ nT. This gives a total uncertainty of 0.5 A for the GIC estimation. Considering the other unknowns such as earthing resistance for the entire network model (Kelly et al., 2017), we argue that this is an acceptable uncertainty for the measured DMM GICs and the best that can be reasonably achieved with a temporary field deployment.

## 3. Measured GICs Using DMM During a G3 Storm

The first set of systems were built and deployed at a site on Whiteadder moor (WHI), eastern Scotland, in June 2018, under the 400 kV line around 15 km west of Torness power station (Figure 2). The system was in operation during the 24–26 August 2018 geomagnetic storm. This G3 event was the largest storm of 2018 with a peak Kp of 7+. The total interplanetary magnetic field reached 21 nT with a prolonged period of southward $B_z$. The storm was possibly caused by a coronal mass ejection from 21 to 22 August 2018, though no classic shock signature was observed. Electric fields peaked at 300 mV/km at Lerwick observatory and 140 mV/km at Eskdalemuir observatory in the east-west component. The HV lines at Whiteadder are linked to Torness substation which has a Hall probe installed to measure GICs directly. This data set, provided by Scottish Power, allows a direct comparison of measured line GICs with data recorded at a nearby substation. This provides an opportunity to validate the DMM and Hall probe measurements with the network model. The three-phase line heights above the sensor in Whiteadder are 12.2, 21.3, and 30.3 m, with the horizontal distance between the wires measured as 18 m. At this site, the sensor was placed under the northernmost circuit.

Figures 3a and 3b show the time series for the two horizontal components of the magnetic field at WHI in geomagnetic coordinates from 25 to 27 August 2018 and the difference between the remote and underline systems. Figures 3c and 3d show the rotation of the horizontal magnetic field measurements into the power line coordinate system (azimuth of 58.7°). The maximum difference between the recordings in the underline and remote magnetometers (in the component transverse to the power line) is ~225 nT. In the component parallel to the power line, the magnetic field differences are close to zero, as expected. This confirms that the measured magnetic field differences arise from currents flowing in the HV line.

Using the simple A-frame pylon model (equation (3) and Figure 1c) and assuming equal current in both circuits, Figure 3e shows an estimated peak-to-peak line current variation of 25 A at 05:13 UT and a second smaller peak of 20 A at 15:58 UT on 26 August. Figure 3f plots the measured line GICs from the Hall probe at Torness substation around 15 km to the east of WHI. Clearly, the shape and structure of the Hall probe signal correlates well with the GIC measurements at Whiteadder (correlation of 0.88), but the amplitude of the Hall probe GICs (maximum of 2 A) is around an order of magnitude smaller.

In order to place these results in context in section 6, we must account for (a) the geoelectric field in the region (see section 4) and (b) the response of the network given the local topology and resistance parameters (see section 5).

## 4. Predicting Electric Field Data Using the MT Impedance Tensor

To reconcile the observed line and Hall probe GIC measurements, we must quantify the electric field strength during storm time. This can be achieved using the electrical conductivity structure which allows the

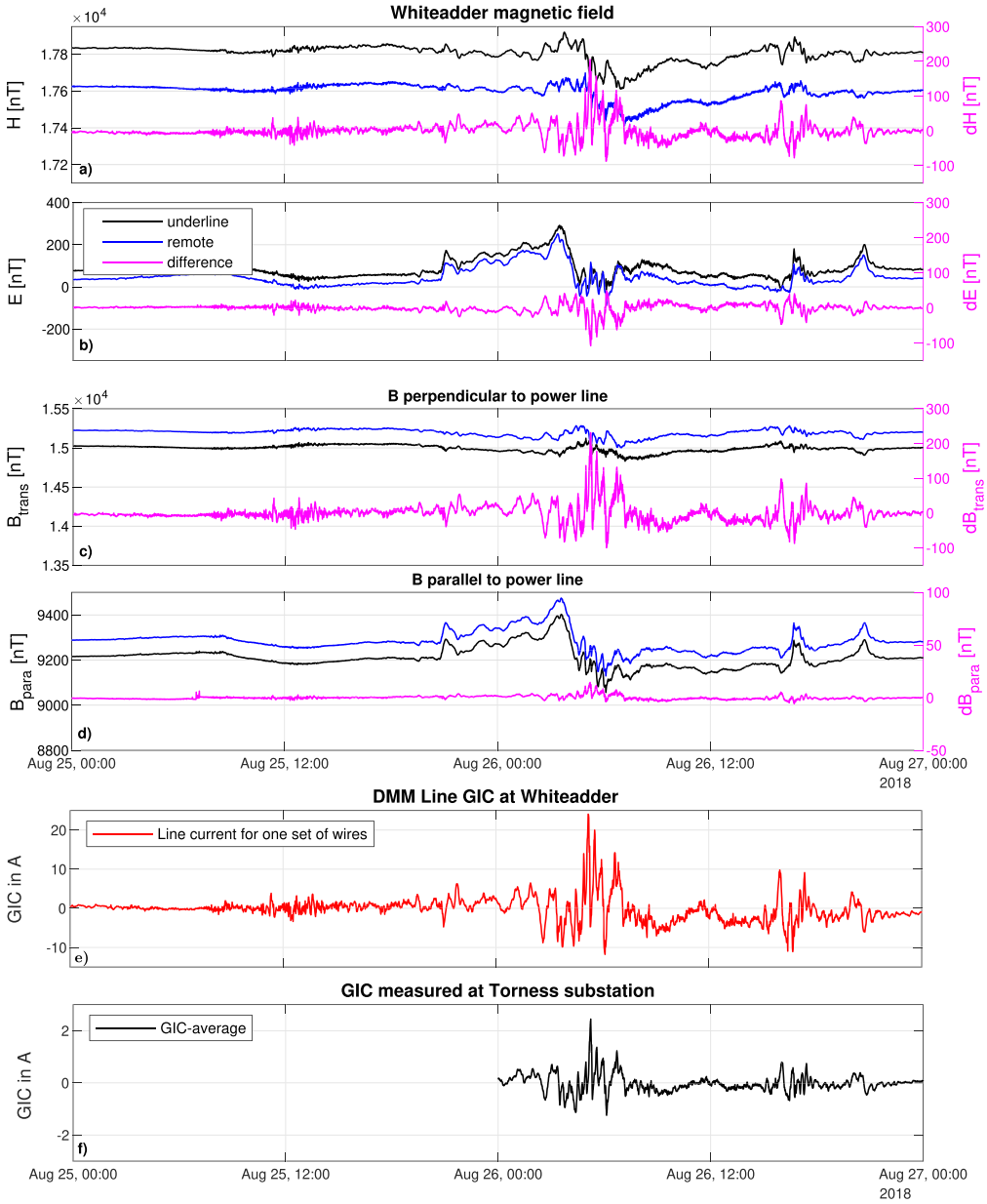


**Figure 3.** Recorded times series during the G3 geomagnetic storm on 25–26 August 2018. (a–d) Horizontal magnetic field components at DMM site Whiteadder, East Lothian (WHI). (e) Line GICs at WHI. (f) GIC data from a Hall probe at Torness substation.

computation of electric fields from measured or interpolated magnetic field variations. Sufficiently detailed electrical conductivity models on the regional scale of a geomagnetic storm are not always readily available. For the British Isles, a thin-sheet model based on bedrock conductivity and airborne near-surface observations is often used to compute the regional geoelectric field (Beamish, 2012; Beggan et al., 2013; Kelly et al., 2017). An alternative way to estimate local electric fields is the use of the MT impedance tensor (Bonner & Schultz, 2017; Campanya et al., 2019; Kelbert et al., 2017), which is defined as the transfer function between electric and magnetic fields at the Earth's surface (Cagniard, 1953). MT is widely used in geophysical deep-sounding exploration and equipment, and processing codes are sophisticated and readily available (Chave & Jones, 2012; Egbert, 1997).

The relationship between electric ($E$) and magnetic fields ($B$) is sought at discrete frequencies $\omega$ through measuring the surface variations of the electric and magnetic fields during quiet times (assuming a plane

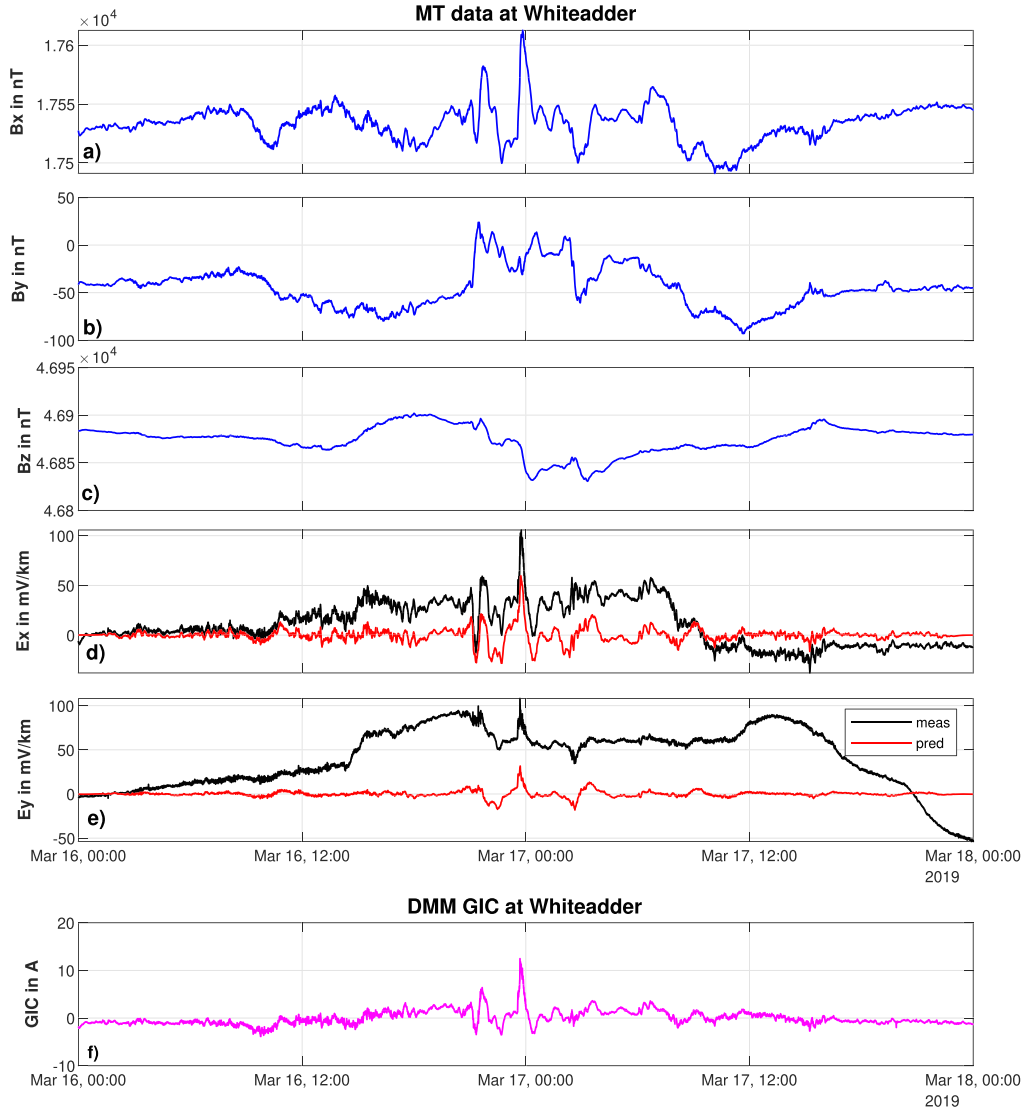


**Figure 4.** Measured magnetic and electric field time series recorded on 16–17 March 2019 and computed line GICs at the Whiteadder (WHI) site. (a–c) Magnetic field, (d, e) electric field, and (f) computed line GICs from DMM measurements.

wave source) and the calculation of the impedance tensor $Z$

$$E(\omega) = Z(\omega) \cdot B(\omega). \tag{4}$$

The tensor $Z$ is assumed to be time independent and contains information about the electrical properties of the subsurface. For space weather applications, it is possible to use this relationship to predict electric fields when magnetic data are available or can be interpolated from nearby observation (e.g., Campanya et al., 2019).

We installed a five-channel Lemi-417 LMT instrument beside the remote magnetometer at Whiteadder for a period of 6 weeks in March–April 2019 (i.e., after the 26 August 2018 storm). The electric field data were of good quality, reflected in small error bars and smooth curves for the robust estimates of the impedance transfer function (see Figure 5). During this period, we recorded data for a minor G1 storm on 16–17 March 2019 (shown in Figure 4). The north component of the electric field (Figure 4d) shows strong correlation with the north component of the magnetic field during the storm and has a maximum amplitude of about 100 mV/km. The line GICs captured with the DMM instruments (Figure 4f) peaks at around 12 A (assuming

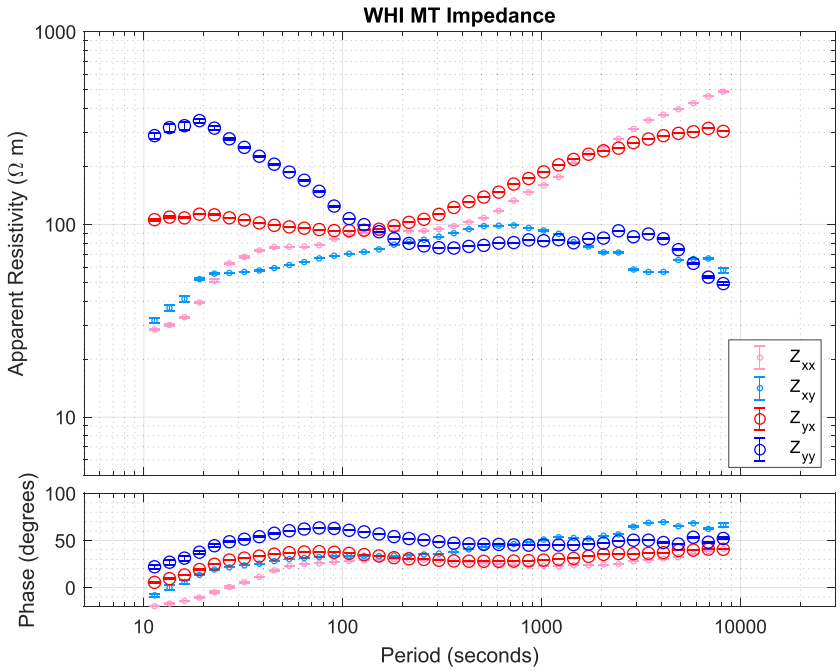


**Figure 5.** Magnetotelluric transfer function for Whiteadder (WHI): Impedance tensor components displayed as apparent resistivity (upper panel) and phase curves (lower panel).

equal GIC flow in each circuit) and closely follows the variation of the electric field, confirming again that the DMM method measures GIC flow due to induced electric fields.

Using 6 weeks of magnetic and electric data, we computed MT transfer functions, after Smirnov (2003). We applied the remote reference technique with the magnetic field variations measured at Eskdalemuir observatory 70 km away to the south (Figure 2) to improve the stability of the transfer functions. The impedance transfer function estimates are stable and smooth between 10 and 10,000 s. Figure 5 shows the transfer function which suggests a complex underlying conductivity structure—likely also indicating the influence of the local coastline.

In order to predict the electric fields using the MT impedance and the magnetic data measured at the site, we take the fast Fourier transform of a 2-day-long segment (with a 1 min sampling rate) and use the resulting Fourier coefficients multiplied by the MT impedance tensor in the frequency domain to compute the spectra of the electric fields before inverting the Fourier transform back into time domain. The uncertainty associated with the violation of the plane wave approximation for storm times depends on the strength of the storm and was estimated as an average SNR value of around 10 dB by Campanya et al. (2019).

To check the consistency of the MT tensor, we computed the estimated electric time series for the March storm (see Figures 4d and 4e). The modeled electric field captures the majority of the measured variations though not the long-period drift or the very short period variation at peak magnitudes. The MT-estimated electric field thus provides a lower minimum value. This is due to the limitation of the frequency range and assumption of a plane wave source when estimating the impedance. Nevertheless, we can now use the MT impedance tensor to compute an estimate of the electric field variation at this location for other time segments if magnetic field time series are available.

## 5. Numerical Modeling of Line and Substation GICs

Over the past two decades, the BGS model of the mainland Britain network has been continuously improved and refined. Starting with McKay (2003) and Turnbull (2010), the basic structure has grown from a 30-node network to 252 nodes and, at present, contains over 1,200 nodes. These nodes represent individual transformers, extracted from the UK National Grid Electricity Ten Year Statement (ETYS) for 2017 (ESO, 2017) allowing for the detailed modeling of GICs in the network. The ETYS gives information regarding the line connections and transformer resistances; the line resistances can be computed from the transmission line

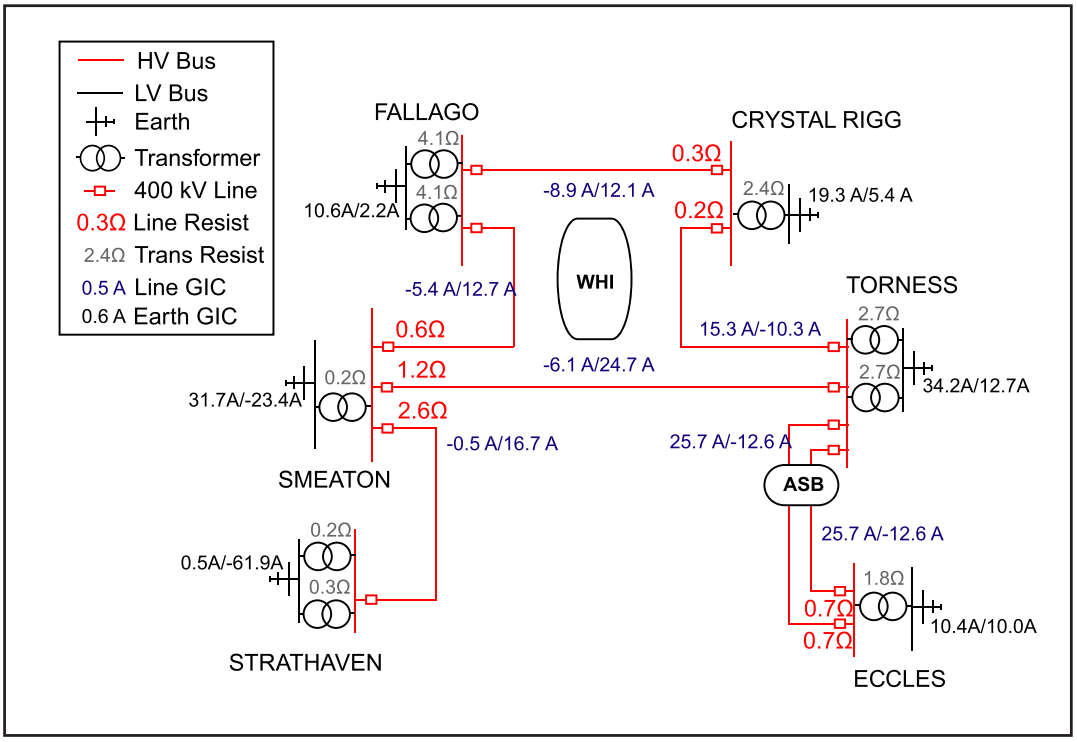


**Figure 6.** Circuit diagram of the partial 400 kV network connected to the Torness substation in Scotland, with modeled line currents (blue text adjacent to the red line) and earthing currents (black text adjacent to substations). Also shown are the line and transformer resistances from 2017 ETYS. The earthing resistance is assumed to be 0.5 Ω. Note that the line currents are GIC per phase, while the earth currents are total GIC through the substation.

impedances expressed as percentage of 100 MVA baseline in the "per-unit" representation (Saadat, 2010). Nonetheless, the publicly available ETYS does not contain all the necessary details for creating a network. For example, the locations of the substations are not precise and the grounding resistances are not included. The substation locations and line paths were found by searching online maps and satellite imagery. The grounding resistances are uniformly set to 0.5 Ω (Kelly et al., 2017).

Figure 6 shows a representation of the circuit diagram for the 400 kV part of the network connected to the Torness substation in East Lothian, Scotland, following the diagrammatic style of Horton et al. (2012). The resistance values (in Ω) of the individual lines (red) and transformers (gray) are derived from the 2017 ETYS. The locations of DMM sites at Whiteadder (WHI) and Abbey St. Bathans (ASB) within the network are indicated on the lines connected to Torness.

The installation at Whiteadder was located under the east-west-orientated 400 kV double circuit running from Torness to Smeaton (Figure 2, inset, and Figure 6). Initially, we have assumed that both circuits connect to the same substations at their end points, for which we computed a peak GIC flow of around 25 A in each circuit (Figure 3). However, in reality, the northern circuit is connected to and grounded at two smaller substations at Fallago and Crystal Rigg which carry power from local wind farms, before arriving at Smeaton (see inset Figure 2). The southern circuit runs directly to Smeaton substation and has a total length of around 50 km in an approximately east-west direction. The GICs in the circuits as they pass the DMM station at Whiteadder are thus unbalanced, and the measured magnetic field is the sum of two different line current magnitudes.

To account for this, we examined the GIC flow in this subset of the network in finer detail. We computed the expected GICs generated by a homogeneous 1 V/km north-south and east-west test electric field. Figure 6 reports the modeled line currents and earthing currents (in amperes). The line current values are displayed as GIC per phase, while the earth currents are the total substation GICs. As a boundary condition check, the total sum of GICs in the network is zero. Note that the 275 and 132 kV parts of the network are included in

the computational model but are not shown on the circuit diagram for clarity (e.g., Smeaton has eight 275 kV transformers).

To interpret the GIC values shown in diagram, note that the line between Fallago and Crystal Rigg has a resistance of 0.3 Ω. Fallago has two 400 kV transformers with resistances of 4.1 Ω each, while Crystal Rigg has a single 400 kV transformer with a lower resistance of 2.4 Ω. For a 1 V/km north-south electric field, a line GIC of 8.9 A per phase is modeled, while 12.1 A per phase flow in an 1 V/km east-west field. At the grounding point in Fallago, a total of 10.6 A flow through the substation for a 1 V/km north-south-orientated field but only 2.2 A for an east-west field. Likewise at Crystal Rigg, 19.3 A flow for a north-south field and 5.4 A for an east-west field.

## 6. Validating the Measured and Modeled GICs at Whiteadder

At the Whiteadder DMM site, modeling of the line GICs suggests that for a 1 V/km east-west electric field, around ($12.1 \times 3 =$) 36.3 A flow in the northern circuit, while the southern circuit carries ($24.7 \times 3 =$) 74.1 A. The total GIC at Torness substation for a 1 V/km north-south field is 34.2 A and 12.7 A for an east-west field. Using the detailed line and transformer model allows us to modify our simple assumptions in equation (2) to compute the GICs and resulting magnetic field created during the geomagnetic storm of 26 August 2018.

We now use the values of the modeled electric field from the MT impedance tensor at Whiteadder to scale the expected GIC flow given by the network model. For example, at the peak of the storm, the modeled electric field at Whiteadder is around 100 mV/km (or 0.1 V/km). Scaling the modeled line GIC gives 3.63 A + 7.41 A, a total of 11.04 A. This equates to a magnetic field value of 150 nT at the DMM underline system.

### 6.1. Comparison of Measurements and Modeling

We compute the line and earthing GICs in a similar manner for each minute of the 26 August 2018 storm. Figure 7 shows a comparison of measured and modeled time series. Figure 7a displays the east-west component of the electric field measured at Eskdalemuir and the values computed at Whiteadder using the MT impedance. Both time series show strong similarity during the storm, with a slightly smaller amplitude of the electric field modeled at Whiteadder. The electric field values were then used to predict the line and earthing GICs and the expected magnetic field difference between the underline and remote systems at WHI. The predicted magnetic field difference closely matches the measured DMM values, though slightly overestimates the amplitude of the signal in Figure 7b (correlation coefficient of 0.67). This produces a very similar time series of modeled and measured line GICs at WHI (in Figure 7c, correlation coefficient of 0.65). Finally, the estimates for the GICs at Torness using the electric field derived from WHI magnetic field measurements (Figure 7d) are slightly larger than the measurements from the Hall probe, particularly at the peak GIC times (correlation coefficient of 0.73).

The results presented in Figure 7 bring together four different sets of measurements and models: the measured DMM magnetic field values, the measured Hall probe GICs, the modeled geoelectric field values from the MT tensor at WHI, and the output of the HV network model. The network model is driven by the electric field from a single point to produce a satisfactory recreation of the measured magnetic field differences at Whiteadder and the GIC data from the Torness Hall probe. The inferred line GICs of up to 20 A along the 400 kV line and the measured value of up to 2 A through the earthing point at Torness can be fully accounted for. This analysis provides the first self-consistent validation of indirectly measured and modeled GICs in a complex HV network.

There remains a mismatch between the amplitude of the modeled and measured GICs for which there are several possible explanations. First, for this initial analysis, we used the local electric field value from Whiteadder. This point measurement might not hold across the entire region. We also computed GICs using electric field data measured at Eskdalemuir which produced a slightly closer match to the Torness GICs than the Whiteadder time series (not shown), suggesting that the electric field is the major source for any difference. Our estimates can be improved by using a regional electric field model. The reasonably good match using a single local electric field estimate suggests that spatial structure of the electric field is relatively homogeneous for this relatively small storm.

Additionally, the actual HV network might have slightly different network parameters (like the earthing resistances) and configuration than used in our model. The HV network is continuously reconfigured to facilitate maintenance or power routing. Finally, the model in Scotland does not yet fully account for the

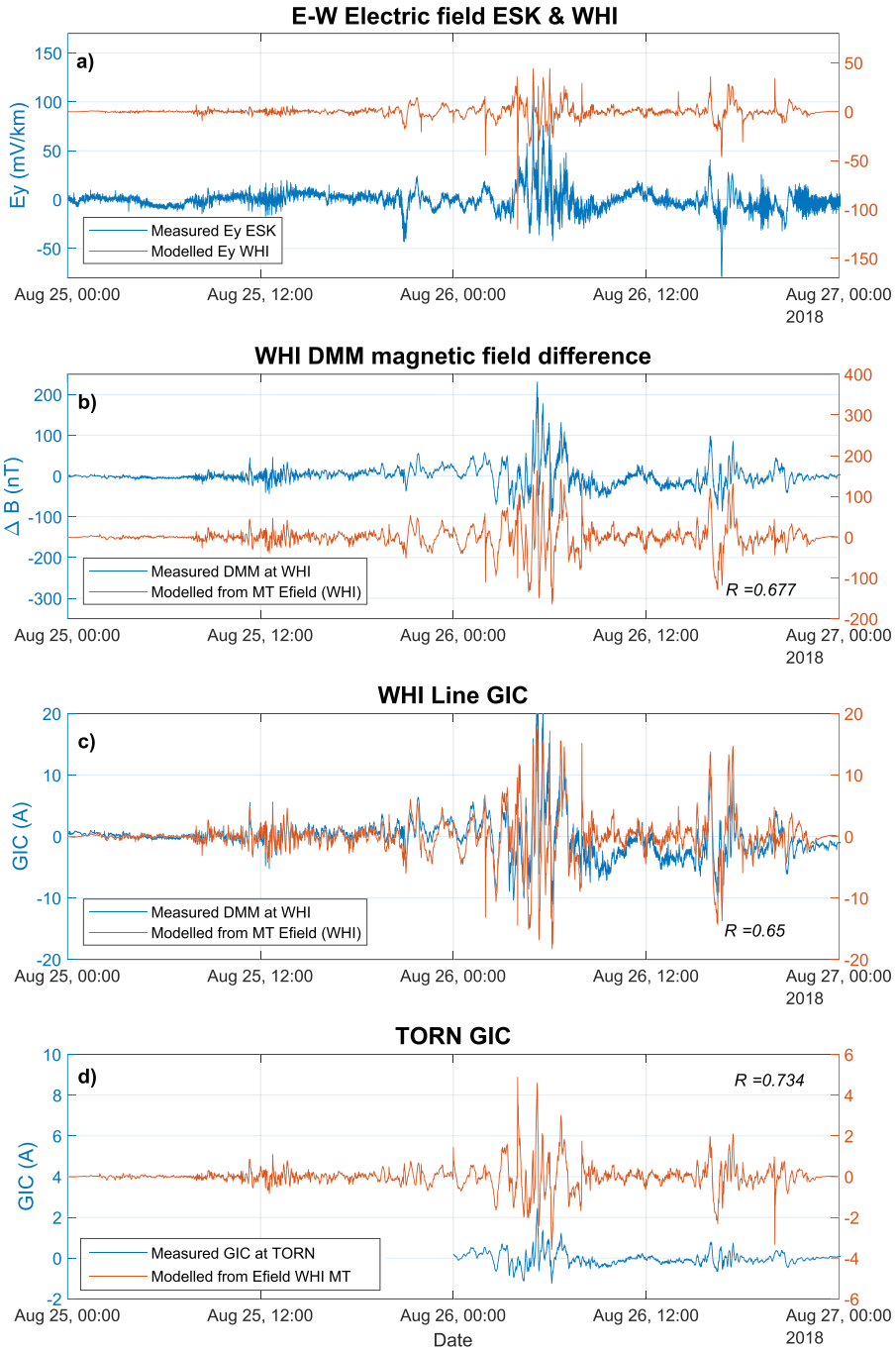


**Figure 7.** Comparison of measured and modeled data: (a) Electric field times series during the G3 geomagnetic storm on 25–27 August 2018 measured at Eskdalemuir and modeled at Whiteadder (WHI), (b) DMM magnetic field differences at WHI, (c) line GICs at site WHI, and (d) GICs at Torness substation with correlation coefficients *R* for the modeled and measured time series.

true length and path of the lines, which adds a few percent uncertainty to the modeled values (e.g., Horton et al., 2012). The true line length and measured grounding values will be addressed in future improvements to the network model.

### 6.2. Reconciling Line and Ground GIC Data

As noted, the measured line GICs at Whiteadder during the 26 August 2018 storm are an order of magnitude larger than the GIC flow through the Hall probe at the Torness substation. The amplitude variation arises

from the different resistance parameters of the network which are traceable through the admittance matrix of the GIC inversion (see also the example in Figure 6). This is modeled by

$$I = (1 + Y \cdot Z)^{-1} \cdot J, \tag{5}$$

where $I$ are the currents at each node, $J$ incorporates the geovoltage between nodes, and $Z$ is the earthing impedance matrix including the earthing resistances of the system. $Y$ is the network admittance matrix (Lehtinen & Pirjola, 1985). The admittance matrix is constructed from the information in the ETYS.

Physically, the 400 kV transformers at Smeaton and Strathaven have a much lower resistance that Fallago, Crystal Rigg, or Torness. This imbalance allows large GICs to flow along the Torness to Smeaton line. At Torness, the GICs are much lower as it presents a more resistive path to ground compared to the other end of the line. Similarly, Fallago and Crystal Rigg substations experience lower GICs because they have higher resistance transformers (>2.4 Ω). The Eccles transformer, connected on a north-south-orientated line, also has a lower resistance (1.8 Ω) than Torness. Therefore, while the lines leading into Torness carry large GICs, the currents cannot readily pass into the ground and are distributed elsewhere. It is thus essential to correctly capture the impedance and admittance information of the network infrastructure in order to accurately model the GIC flow. Without this level of detail, it would be easily possible to produce a plausible, though incorrect, assessment of GIC hazard within a poorly described network.

## 7. Conclusions

We present the design and initial deployment of the first DMM systems in the United Kingdom. In this study we focus on the measurements from the first site installed at Whiteadder in eastern Scotland. At this site we have successfully detected GICs in a 400 kV HV power network. The line GIC data recorded at Whiteadder during the 26 August 2018 storm were compared to data from a Hall probe at the nearby substation at Torness. The measured GICs from the line and the Hall probe show excellent temporal correlation, though with significant differences in amplitude, illustrating that line measurements with DMM and Hall probes at grounding points capture different but complementary views of GIC flow in a network.

Using the latest model of the HV network and electric field variations estimated from an MT survey, we show that the measured line and earthing GICs match the expected modeled values during the geomagnetic storm. This analysis assimilates four different sets of measurements and modeling, the measured DMM magnetic field values, the measured Hall probe GICs, the modeled geoelectric field values from the MT tensor at WHI, and the output of the HV network model to provide a self-consistent validation of the BGS HV network model using measured data. This is the first study to validate such a complex network model using direct and indirect measurements of GICs. The remaining differences between measured and modeled values can be ascribed to the use of the electric field estimated at a single location, likely errors in the network grounding resistance parameters and incomplete information about the network configuration.

Improved modeling of the electric field in conjunction with a more detailed network representation should lead iteratively to a better fit between the modeled GICs and observations. The data collected by the DMM systems will be a vital part of making those improvements. We will continue to use the DMM measurements to collect GIC data across the United Kingdom to validate and refine numerical modeling of the GICs across the entire network and improve the modeling of the electric field.

**Acknowledgments**
We wish to thank the BGS Geomagnetism engineering team (Tony Swan, Tim Taylor, and Chris Turbitt) for their work in designing, procuring, building, and testing the differential magnetometer equipment and providing fieldwork assistance. We thank the landowners who granted access for installing DMM equipment. We also thank Scottish Power Ltd. for providing Hall probe data at Torness substation and Colin Hogg at Dublin Institute for Advanced Studies for the loan of the long-period magnetotelluric (LMT) instrument. This work is funded under UK Natural Environment Research Council Grant NE/P017231/1 "Space Weather Impact on Ground-based Systems (SWIGS)." DMM data and the MT transfer function for station WHI are available in the supporting information; all data collected within the SWIGS project will be openly available from the National Geoscience Data Centre (https://www.bgs.ac.uk/services/ngdc/) in 2021. Torness GIC data are available on request from Scottish Power Ltd. This paper is published with the permission of the Executive Director of the British Geological Survey (UKRI).

## References

Albertson, V. D., Kappenman, J. G., Mohan, N., & Skarbakka, G. A. (1981). Load-flow studies in the presence of geomagnetically-induced currents. *IEEE Transactions on Power Apparatus and Systems*, *PAS-100*(2), 594–607. https://doi.org/10.1109/TPAS.1981.316916

Bailey, R. L., Halbedl, T. S., Schattauer, I., Achleitner, G., & Leonhardt, R. (2018). Validating GIC models with measurements in Austria: Evaluation of accuracy and sensitivity to input parameters. *Space Weather*, *16*(7), 887–902. https://doi.org/10.1029/2018SW001842

Beamish, D. (2012). The 1:625k near-surface bedrock electrical conductivity map of the UK (Tech. Rep. No. OR/12/037). British Geological Survey. http://nora.nerc.ac.uk/20833/

Beamish, D., Clark, T. D. G., Clarke, E., & Thomson, A. W. P. (2002). Geomagnetically induced currents in the UK: Geomagnetic variations and surface electric fields. *Journal of Atmospheric and Solar-Terrestrial Physics*, *64*, 1779–1792. https://doi.org/10.1016/S1364-6826(02)00127-X

Beggan, C. D. (2015). Sensitivity of geomagnetically induced currents to varying auroral electrojet and conductivity models. *Earth, Planets and Space*, *67*(1), 1–12. https://doi.org/10.1186/s40623-014-0168-9

Beggan, C. D., Beamish, D., Richards, A., Kelly, G. S., & Thomson, A. W. P. (2013). Prediction of extreme geomagnetically induced currents in the UK high-voltage network. *Space Weather*, *11*, 407–419. https://doi.org/10.1002/swe.20065

Blake, S. P., Gallagher, P. T., Campanyá, J., Hogg, C., Beggan, C. D., Thomson, A. P., et al. (2018). A detailed model of the Irish high voltage power network for simulating GICs. *Space Weather*, *16*, 1770–1783. https://doi.org/10.1029/2018SW001926

Bolduc, L. (2002). GIC observations and studies in the Hydro-Québec power system. *Journal of Atmospheric and Solar-Terrestrial Physics*, *64*, 1793–1802. https://doi.org/10.1016/S1364-6826(02)00128-1

Bonner, L. R., & Schultz, A. (2017). Rapid prediction of electric fields associated with geomagnetically induced currents in the presence of three-dimensional ground structure: Projection of remote magnetic observatory data through magnetotelluric impedance tensors. *Space Weather*, *15*, 204–227. https://doi.org/10.1002/2016SW001535

Boteler, D. H. (2006). The super storms of August/September 1859 and their effects on the telegraph system. *Advances in Space Research*, *38*(2), 159–172. https://doi.org/10.1016/j.asr.2006.01.013

Boteler, D. H. (2019). A 21st century view of the March 1989 magnetic storm. *Space Weather*, *17*, 1427–1441. https://doi.org/10.1029/2019SW002278

Boteler, D. H., & Pirjola, R. J. (2014). Comparison of methods for modelling geomagnetically induced currents. *Annales Geophysicae*, *32*(9), 1177–1187. https://doi.org/10.5194/angeo-32-1177-2014

Butala, M. D., Kazerooni, M., Makela, J. J., Kamalabadi, F., Gannon, J. L., Zhu, H., & Overbye, T. J. (2017). Modeling geomagnetically induced currents from magnetometer measurements: Spatial scale assessed with reference measurements. *Space Weather*, *15*, 1357–1372. https://doi.org/10.1002/2017SW001602

Cagniard, L. (1953). Basic theory of the magnetotelluric method of geophysical prospecting. *Geophysics*, *18*, 605–635. https://doi.org/10.1190/1.1437915

Campanya, J., Gallagher, P. T., Blake, S. P., Gibbs, M., Jackson, D., Beggan, C. D., et al. (2019). Modeling geoelectric fields in Ireland and the UK for space weather applications. *Space Weather*, *17*, 216–237. https://doi.org/10.1029/2018SW001999

Campbell, W. H. (1980). Observation of electric currents in the Alaskan oil pipeline resulting from auroral electrojet current sources. *Geophysical Journal of the Royal Astronomical Society*, *61*, 437–449. https://doi.org/10.1111/j.1365-246X.1980.tb04325.x

Chave, A. D., & Jones, A. G. (2012). *The magnetotelluric method: Theory and practice*. Cambridge: Cambridge University Press. https://doi.org/10.1017/CBO9781139020138

Clilverd, M. A., Rodger, C. J., Brundell, J. B., Dalzell, M., Martin, I., Mac Manus, D. H., et al. (2018). Long-lasting geomagnetically induced currents and harmonic distortion observed in New Zealand during the 7-8 September 2017 disturbed period. *Space Weather*, *16*, 704–717. https://doi.org/10.1029/2018SW001822

Divett, T., Richardson, G. S., Beggan, C. D., Rodger, C. J., Boteler, D. H., Ingham, M., et al. (2018). Transformer-level modeling of geomagnetically induced currents in New Zealand's South Island. *Space Weather*, *16*, 718–735. https://doi.org/10.1029/2018SW001814

ESO, N. G. (2017). Electricity Ten Year Statement 2017 (Tech. Rep.). https://www.nationalgrideso.com/publications/electricity-ten-year-statement-etys

Egbert, G. D. (1997). Robust multiple-station magnetotelluric data processing. *Geophysical Journal International*, *130*(2), 475–496. https://doi.org/10.1111/j.1365-246X.1997.tb05663.x

FDSN (2012). SEED reference manual, Standard for the exchange of earthquake data, SEED format version 2.4. Computer software manual.

Horton, R., Boteler, D., Overbye, T. J., Pirjola, R., & Dugan, R. C. (2012). A test case for the calculation of geomagnetically induced currents. *IEEE Transactions on Power Delivery*, *27*(4), 2368–2373. https://doi.org/10.1109/TPWRD.2012.2206407

Kelbert, A., Balch, C. C., Pulkkinen, A., Egbert, G. D., Love, J. J., Rigler, E. J., & Fujii, I. (2017). Methodology for time-domain estimation of storm time geoelectric fields using the 3-D magnetotelluric response tensors. *Space Weather*, *15*, 874–894. https://doi.org/10.1002/2017SW001594

Kelly, G. S., Viljanen, A., Beggan, C. D., & Thomson, A. W. P. (2017). Understanding GIC in the UK and French high-voltage transmission systems during severe magnetic storms. *Space Weather*, *15*, 99–114. https://doi.org/10.1002/2016SW001469

Lehtinen, M., & Pirjola, R. (1985). Currents produced in earthed conductor networks by geomagnetically-induced electric fields. *Annales Geophysicae*, *4*, 479–484.

Love, J. J., Lucas, G. M., Kelbert, A., & Bedrosian, P. A. (2018). Geoelectric hazard maps for the Mid-Atlantic United States: 100 year extreme values and the 1989 magnetic storm. *Geophysical Research Letters*, *45*, 5–14. https://doi.org/10.1002/2017GL076042

Mac Manus, D. H., Rodger, C. J., Dalzell, M., Thomson, A. W. P., Clilverd, M. A., Petersen, T., et al. (2017). Long-term geomagnetically induced current observations in New Zealand: Earth return corrections and geomagnetic field driver. *Space Weather*, *15*, 1020–1038. https://doi.org/10.1002/2017SW001635

Marshall, R. A., Dalzell, M., Waters, C. L., Goldthorpe, P., & Smith, E. A. (2012). Geomagnetically induced currents in the New Zealand power network. *Space Weather*, *10*, S08003. https://doi.org/10.1029/2012SW000806

Matandirotya, E., Cilliers, Pierre. J., Van Zyl, R. R., Oyedokun, D. T., & de Villiers, J. (2016). Differential magnetometer method applied to measurement of geomagnetically induced currents in Southern African power networks. *Space Weather*, *14*, 221–232. https://doi.org/10.1002/2015SW001289

McKay, A. (2003). Geoelectric fields and geomagnetically induced currents in the United Kingdom (Doctoral dissertation), University of Edinburgh. https://era.ed.ac.uk/bitstream/handle/1842/639/allanmckthesis.pdf?sequence=2&isAllowed=y

Myllys, M., Viljanen, A., Rui, O. A., & Ohnstad, T. M. (2014). Geomagnetically induced currents in Norway: The northernmost high-voltage power grid in the world. *Journal of Space Weather and Space Climate*, *4*, 8. https://doi.org/10.1051/swsc/2014007

Oughton, E. J., Hapgood, M., Richardson, G. S., Beggan, C. D., Thomson, A. W. P., Gibbs, M., et al. (2018). A risk assessment framework for the socioeconomic impacts of electricity transmission infrastructure failure due to space weather: An application to the United Kingdom. *Risk Analysis*, *38*(12), 1–22. https://doi.org/10.1111/risa.13229

Oughton, E. J., Skelton, A., Horne, R. B., Thomson, A. W. P., & Gaunt, C. T. (2017). Quantifying the daily economic impact of extreme space weather due to failure in electricity transmission infrastructure. *Space Weather*, *15*, 65–83. https://doi.org/10.1002/2016SW001491

Pulkkinen, A., Bernabeu, E., Eichner, J., Beggan, C., & Thomson, A. (2012). Generation of 100-year geomagnetically induced current scenarios. *Space Weather*, *10*, S04003. https://doi.org/10.1029/2011SW000750

Pulkkinen, A., Viljanen, A., Pajunpaa, K., & Pirjola, R. (2001). Recordings and occurrence of geomagnetically induced currents in the Finnish natural gas pipeline network. *Journal of Applied Geophysics*, *48*(4), 219–231. https://doi.org/10.1016/S0926-9851(01)00108-2

Pulkkinen, A., Viljanen, A., & Pirjola, R. (2006). Estimation of geomagnetically induced current levels from different input data. *Space Weather*, *4*, S08005. https://doi.org/10.1029/2006SW000229

Rosenqvist, L., & Hall, J. O. (2019). Regional 3-D modeling and verification of geomagnetically induced currents in Sweden. *Space Weather*, *17*, 27–36. https://doi.org/10.1029/2018SW002084

Saadat, H. (2010). *Power system analysis* (3rd ed.). Mcgraw-Hill College: PSA Publishing LLC.

Smirnov, M. (2003). Magnetotelluric data processing with a robust statistical procedure having a high breakdown point. *Geophysical Journal International*, *152*(1), 1–7. https://doi.org/10.1046/j.1365-246X.2003.01733.x

Thomson, A. W. P., McKay, A. J., Clarke, E., & Reay, S. J. (2005). Surface electric fields and geomagnetically induced currents in the Scottish Power grid during the 30 October 2003 geomagnetic storm. *Space Weather*, *3*, S11002. https://doi.org/10.1029/2005SW000156

Torta, J. M., Marcuello, A., Campanyá, J., Marsal, S., Queralt, P., & Ledo, J. (2017). Improving the modeling of geomagnetically induced currents in Spain. *Space Weather*, *15*, 691–703. https://doi.org/10.1002/2017SW001628

Turnbull, K. (2010). Modelling GIC in the UK. *Astronomy & Geophysics*, *51*(5), 25–26. https://doi.org/10.1111/j.1468-4004.2010.51525.x

Viljanen, A., & Pirjola, R. (1994). Geomagnetically induced currents in the Finnish high-voltage power system. *Surveys in Geophysics*, *15*(4), 383–408. https://doi.org/10.1007/BF00665999

Viljanen, A., Pirjola, R., Prácser, E., Katkalov, J., & Wik, M. (2014). Geomagnetically induced currents in Europe—Modelled occurrence in a continent-wide power grid. *Journal of Space Weather and Space Climate*, *4*, 9. https://doi.org/10.1051/swsc/2014006